Conversion of Li2FeSbO5 to the Fe(III)/Fe(V) Phase LiFeSbO5 via Topochemical Lithium Extraction

MARTÍNEZ DE IRUJO-LABALDE, X, SCRIMSHIRE, Alex <http://orcid.org/0000-0002-6828-3620>, BINGHAM, Paul <http://orcid.org/0000-0001-6017-0798>, SUARD, E <http://orcid.org/0000-0001-5966-5929> and HAYWARD, MA <http://orcid.org/0000-0002-6248-2063>

Conversion of Li_2FeSbO_5 to the Fe(III)/Fe(V) phase $LiFeSbO_5$ via topochemical lithium extraction.

Xabier Martínez de Irujo-Labalde[†ψ], Alex Scrimshire [‡], Paul A. Bingham [‡], Emmanuelle Suard[§] and
Michael A. Hayward[†ψ] *.

[†] Department of Chemistry, University of Oxford, Inorganic Chemistry Laboratory, South Parks Road, Oxford, OX1 3QR, UK.

[ψ] The Faraday Institution, Quad One, Harwell Campus, Didcot, OX11 0RA, UK.

[‡] Materials and Engineering Research Institute, Sheffield Hallam University, City Campus, Howard Street, Sheffield, S1 1WB, UK.

[§]Institut Laue Langevin (ILL), Grenoble 9 F-38042, France.

ABSTRACT: Reaction between Na_2FeSbO_5 and $LiNO_3$ at 300 °C yields the metastable phase Li_2FeSbO_5 which is isostructural with the sodium 'parent' phase (space group *Pbna*, a = 15.138(1) Å, b = 5.1440(3) Å, c = 10.0936(6) Å) consisting of an alternating stack of $Li_2Fe_2O_5$ and $Li_2Sb_2O_5$ sheets containing tetrahedral coordinated Fe^{3+} and octahedrally coordinated Sb^{5+} respectively. Further reaction between Li_2FeSbO_5 with NO_2BF_4 in acetonitrile at room temperature yields $LiFeSbO_5$ which adopts an orthorhombic structure (space group $Pbn2_1$, a = 14.2943(4) Å, b = 5.2771(1) Å, c = 9.5610(3) Å) in which the $LiFeO_5$ layers have shifted on lithium extraction resulting in an octahedral coordination for the iron cations. ^{57}Fe Mössbauer data indicate that the nominal Fe^{4+} cations present in $LiFeSbO_5$ have disproportionated into a 1:1 combination of Fe^{3+} and Fe^{5+} centers which are ordered within the $LiFeSbO_5$ structural framework. It is widely observed that Fe^{4+} centers tend to be unstable in de-lithiated Li-Fe-X-O phases currently proposed as lithium-ion battery cathode materials, so the apparent stability of highly oxidized Fe^{5+} centers in $LiFeSbO_5$ is notable, suggesting cathode materials based on oxidizing Fe^{3+} could be possible. However, in this instance, the structural change which occurs on delithiation of Li_2FeSbO_5 prevents electrochemical cycling of this material.

Introduction

Rechargeable lithium-ion batteries have become the power source of choice for a wide variety of technologies from personal electronic devices to electric vehicles. However, the majority of cathode materials used in high-voltage batteries rely on rare, expensive and toxic elements, such as cobalt, nickel and manganese for their energy storage performance.[1-3] If lithium-ion batteries are to be utilized widely in transport applications or as energy stores for renewable power generation, the use of these elements will need to be minimized.[4, 5]

In principle, utilizing iron in lithium-ion battery cathodes materials looks like an attractive prospect, due to the high abundance, low cost, and low toxicity of iron compounds.[6] However, while it has been possible to make use of the $Fe^{II/III}$ couple in cathodes such as $LiFePO_4$,[7] utilizing the $Fe^{III/IV}$ couple in high-voltage cathodes with an enduring high capacity, has proved challenging.

For example, $LiFeO_2$ can be prepared with a number of different crystal structures,[8, 9] but none of these materials exhibit good, long-term electrochemical performance. The most stable form at high temperature, α-$LiFeO_2$,[10, 11] adopts a disordered rock salt structure which exhibits slow lithium intercalation/deintercalation kinetics unless prepared in nanoparticulate form [12, 13] – a feature shared by cation-ordered γ-$LiFeO_2$,[14, 15] which is the most stable polymorph at room temperature.[10] By utilizing low-temperature synthesis approaches, metastable forms of $LiFeO_2$ can be prepared such as the 'corrugated layer' phase synthesized by reaction of γ-FeOOH and LiOH,[9, 16] or the 'O3'-$LiFeO_2$ or t-$LiFeO_2$ polymorphs prepared via Li-for-Na cation exchange from α-$NaFeO_2$ and β-$NaFeO_2$ respectively.[17, 18] These low-temperature forms of $LiFeO_2$ can show appreciable electrochemical activity, however detailed analysis reveals that during the first lithium deintercalation cycle these materials, along with α-$LiFeO_2$ and γ-$LiFeO_2$, are converted to the spinel $LiFe_5O_8$,[11, 18-21] with subsequent electrochemical activity most likely due to cycling between $LiFe_5O_8$ and $Li_3Fe_5O_8$.[22] Furthermore, post-cycling analysis casts doubt on the stability of Fe^{4+} in the Li-Fe-O system, with either rapid loss of oxygen or reaction with the electrolyte occurring in tandem with the initial removal of lithium.[18, 21, 23]

Similar instabilities of the Fe^{4+} oxidation state have been observed in other Li-Fe-X-O systems, with anion-redox process observed on lithium extraction.[24, 25] For example, the extraction of a single lithium from Li_2FeSiO_4 is associated with the oxidation of Fe^{2+} to Fe^{3+}. However, removal of a second lithium is accompanied by the formation of 'ligand holes' in the O-2p bands, although this does not ap-

pear to lead to oxygen release.[26] Conversely, lithium extraction from Li_4FeSbO_6 leads to oxidation of both Fe^{3+} and oxygen, with the former being reversible, but the anion oxidation being apparently irreversible.[27, 28]

Here we describe the synthesis of another Li-Fe-Sb-O phase, Li_2FeSbO_5, via cation exchange from Na_2FeSbO_5.[29, 30] Oxidative lithium extraction from Li_2FeSbO_5 occurs via oxidation of Fe^{3+}, however in this instance the Fe^{4+} cations nominally present in $LiFeSbO_5$ disproportionate into a 1:1 mixture of Fe^{3+} and Fe^{5+}.

Experimental

Synthesis. Polycrystalline samples of Na_2FeSbO_5 were synthesized by a high-temperature ceramic method. Suitable ratios of Fe_2O_3 (Alfa Aesar, 99.995%), Sb_2O_3 (Alfa Aesar, 99.999%) and a 5% excess of Na_2CO_3 (Alfa Aesar, 99.95%) were ground together using an agate pestle and mortar. These mixtures were placed an alumina crucibles and heated in air at 600 °C for 12 hours. The powders were reground, pressed into 13 mm pellets, and then heated at 1050 °C for 4 periods of 12 hours in air with intermediate grindings. X-ray powder diffraction data collected from samples of Na_2FeSbO_5 prepared in this way yielded lattice parameters of (a = 15.7202(1) Å, b = 5.3250(1) Å, c = 10.8950(1) Å) consistent with previous reports.[29, 30]

Li-for-Na cation exchange of Na_2FeSbO_5 was achieved by heating samples at 300 °C with 10 mole equivalents of $LiNO_3$ (Alfa Aesar, 99%) for 3 days. The resulting material was then washed with distilled water to remove the $NaNO_3$ and excess $LiNO_3$ and then dried for 12 hours at 140 °C in air.

Attempts to oxidatively remove Li from Li_2FeSbO_5 were performed using NO_2BF_4, a reagent with very strong oxidizing character (5.1V vs Li/Li^+).[31] 200 mg of Li_2FeSbO_5 was suspended in a solution of 1g of NO_2BF_4 (Sigma Aldrich. 95%) in 10 ml of acetonitrile (Merck, 99.8%). The suspension was stirred under N_2 for 2 days at room temperature. The material was then filtered and washed repeatedly with clean acetonitrile under inert atmosphere before being dried under vacuum.

Reintercalation of lithium into $Li_{2-x}FeSbO_5$ was attempted by stirring samples in acetonitrile with LiI at 50 °C for two days. There was no iodine formed in this process, indicating the deinterclation reaction is not readily reversible.

Characterization. Reaction progress and initial structural characterization was performed using laboratory X-ray powder diffraction (PXRD) data collected using a PANalytical X'pert diffractometer incorporating an X'celerator position-sensitive detector (monochromatic Cu Kα1 radiation). High-resolution synchrotron X-ray powder diffraction (SXRD) data were collected using the I11 instrument at the Diamond Light Source Ltd. Diffraction patterns were collected using Si-calibrated X-rays with an approximate wavelength of 0.825 Å from samples, sealed in 0.3 mm diameter borosilicate glass capillaries. Neutron powder diffraction (NPD) data were collected using the D2B diffractometer (λ = 1.594 Å) at the ILL neutron source, from samples contained within vanadium cans. Rietveld refinement of powder diffraction data was performed using the TOPAS Academic (V6).[32]

^{57}Fe Mössbauer spectroscopy measurements utilized acrylic absorber discs with a sample area of 1.767 cm^2 which were loaded to present 2.16 × 10^{-3} g cm^{-2} of Fe, and achieve a Mössbauer thickness of 1. Samples were homogeneously mixed with graphite to achieve this level of loading. The 14.4 keV γ-rays were supplied by the cascade decay of 25 mCi ^{57}Co in a Rh matrix source, oscillated at constant acceleration by a SeeCo W304 drive unit, and detected using a SeeCo 45431 Kr proportional counter operating with 1.745 kV bias voltage applied to the cathode. All measurements were calibrated relative to α-Fe foil. Spectral data were fitted using the Recoil software package,[33] using Lorentzian line shapes. Thermogravimetric measurements were performed by heating powder samples at a rate of 5 °C min^{-1} under flowing air, using a Mettler-Toledo MX1 thermogravimetric microbalance, and then cooling to 25 °C. DC magnetization data were collected using a Quantum Design MPMS SQUID magnetometer from samples contained in gelatine capsules.

Results

Structural characterization of Li_2FeSbO_5. Direct synthesis of Li_2FeSbO_5 from Li_2CO_3, Fe_2O_3 and Sb_2O_3 was not possible, with the reaction between these reagents resulting in mixtures of $LiSbO_3$ and $LiFe_{1-x}Sb_xO_2$. However, reaction between Na_2FeSbO_5 and $LiNO_3$, as described above, yields a crystalline material. SXRD data collected from this material can be indexed using an orthorhombic unit cell (a = 15.138(1) Å, b = 5.1440(3) Å, c = 10.0936(6) Å) with extinction conditions consistent with space group *Pbna* and with diffraction peak intensities similar to the Na_2FeSbO_5 parent phase (Figure 1), suggesting a simple Li-for-Na cation exchange has occurred. The widths of the diffraction peaks of Li_2FeSbO_5 are broader than those of Na_2FeSbO_5 (Figure 1) consistent with a smaller particle size/reduced crystallinity in the cation exchanged material. A model based on the reported structure of Na_2FeSbO_5 (space group *Pbna*),[29] but with the Na cations replaced by Li, was refined against NPD data collected from the cation-exchanged material at room temperature, to achieve a good fit to the data, as shown in Figure 2. Refinement of the Li-site occupancies did not result in deviations from unity, within error. Given the strong neutron scattering contrast between Li (-1.90 fm) and Na (3.63 fm),[34] this suggests complete cation exchange has occurred, and the exchanged phase has a composition of Li_2FeSbO_5, within the sensitivity of our measurements. Details of the refined model of Li_2FeSbO_5 are given in Table 1, with selected bond lengths in Table S1 in the supporting information.

Structural and compositional characterization of chemically delithiated Li_2FeSbO_5. Reaction between Li_2FeSbO_5 and NO_2BF_4, as described above, yields a further

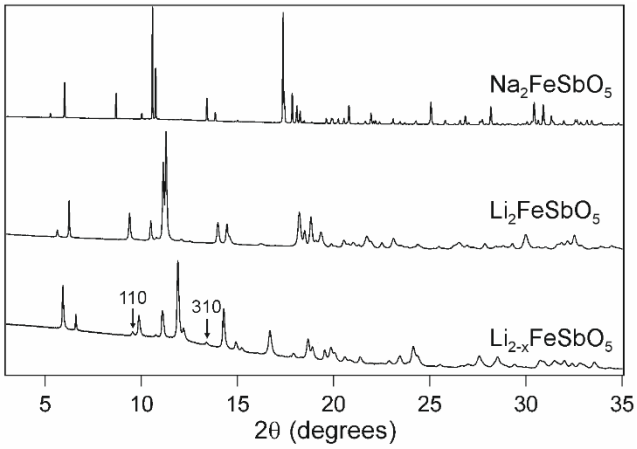

Figure 1. SXRD data collected at room temperature from Na_2FeSbO_5 (top) and Li_2FeSbO_5 (middle) and $Li_{2-x}FeSbO_5$ (bottom).

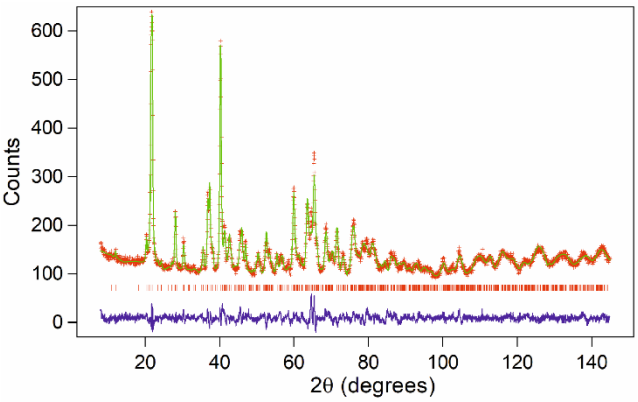

Figure 2. Observed, calculated and difference plots from the structural refinement of Li_2FeSbO_5 against NPD data collected at room temperature.

crystalline material. SXRD data collected from this material can be indexed using an orthorhombic unit cell with dimensions similar to the parent Li_2FeSbO_5 phase (a = 14.2943(4) Å, b = 5.2771(1) Å, c = 9.5610(3) Å).

The chemical composition of the delithiated phase was determined by thermogravimetric analysis. A sample of $Li_{2-x}FeSbO_5$ was heated in air to 1000 °C and observed to lose 8.31% of its mass. PXRD data collected from the product of this process indicated the $Li_{2-x}FeSbO_5$ had decomposed to a mixture of $FeSbO_4$, $LiSbO_3$ and $LiFe_2SbO_6$. Combining these observations we determined the initial composition of the delithiated phase was $Li_{0.99(5)}FeSbO_5$, as described in detail in the supporting information. This phase will henceforth be referred to as $LiFeSbO_5$.

Close inspection of the SXRD data collected from $LiFeSbO_5$ reveals the presence of the [110] and [310] reflections (Figure 1) which violate the *hk*o: $h = 2n$ extinction condition of the *Pbna* space group used to describe the structure of Li_2FeSbO_5. Specifically the conditions associated with the *a*-glide are violated, which suggests a symmetry lowering to either *Pbnm* (# 62) or $Pbn2_1$ (#33).

Atom	Site	x	y	z	B_{eq} (Å²)
Li(1)	4*c*	0.120(2)	0.75	0.5	0.73(1)
Li(2)	4*c*	0.462(2)	0.25	0.5	0.81(4)
Li(3)	8*d*	0.334(1)	0.333(3)	0.761(2)	0.96(5)
Sb(1)	4*c*	0.235(1)	0.25	0.5	0.83(2)
Sb(2)	4*c*	0.341(1)	0.75	0.5	0.86(2)
Fe(1)	8*d*	0.947(4)	0.752(1)	0.2926(5)	0.33(7)
O(1)	8*d*	0.1458(7)	0.093(2)	0.606(1)	0.94(2)
O(2)	8*d*	0.3316(8)	0.051(2)	0.599(1)	0.44(2)
O(3)	8*d*	0.4431(8)	0.867(2)	0.3890(9)	1.03(2)
O(4)	8*d*	0.2498(7)	0.933(2)	0.388(1)	0.55(2)
O(5)	8*d*	0.0548(7)	0.925(2)	0.3422(7)	0.75(2)
Li_2FeSbO_5 – space group *Pbna* (#60)					
a = 15.138(1) Å, b = 5.1440(3) Å c = 10.0936(6) Å,					
volume = 786.01(8) Å³					
Formula weight = 271.48 g mol⁻¹, Z = 8					
Radiation source: Neutron, λ = 1.594 Å					
Temperature: 298 K					
R_p = 3.38 %, R_{wp} = 4.30 %, R_{Bragg} = 1.19					

Table 1. Parameters from the structural refinement of Li_2FeSbO_5 against NPD data collected at room temperature.

A series of structural models were constructed in space groups *Pbnm* and $Pbn2_1$, with the assistance of the ISODISTORT software package.[35, 36] Lithium positions were omitted from these models, as these ions do not contribute significantly to the X-ray diffraction data due to their small X-ray scattering power. A structural model constructed in space group $Pbn2_1$ which conserved the positions of the octahedrally coordinated Sb^{5+} cations from the Li_2FeSbO_5 parent phase, but located the Fe cations in octahedral sites, fit the data well. Initially the model was constrained to force the two crystallographically distinct Sb sites to be identical. However, this constraint was relaxed in later refinement cycles, leading to an improvement in the fit to the data (Figure 3). Full details of the refined structure of $LiFeSbO_5$ are given in Table 2, with selected bond lengths in Table S2 in the supporting information.

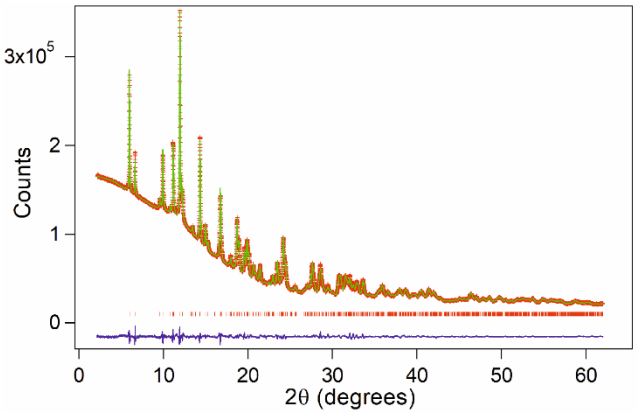

Figure 3. Observed, calculated and difference plots from the structural refinement of $LiFeSbO_5$ against SXRD data collected at room temperature.

	Site	x	y	z	B_{eq} (Å²)
Sb(1)	4*a*	0.4978(1)	0.1365(1)	0	0.22(2)
Sb(2)	4*a*	0.8932(1)	0.1364(1)	0.9942(1)	0.22(2)
Fe(1)	4*a*	0.6916(1)	0.1040(1)	0.7431(1)	0.28(1)
Fe(2)	4*a*	0.6955(1)	0.8657(1)	0.2538(1)	0.28(1)
O(1)	4*a*	0.0840(23)	0.7855(18)	0.8928(17)	0.48(2)
O(2)	4*a*	0.0994(8)	0.5779(17)	0.1522(13)	0.48(2)
O(3)	4*a*	0.9031(9)	0.7910(20)	0.8478(16)	0.48(2)
O(4)	4*a*	0.8993(10)	0.4508(17)	0.1165(18)	0.48(2)
O(5)	4*a*	0.7040(8)	0.5779(17)	0.1080(11)	0.48(2)
O(6)	4*a*	0.6889(9)	0.7855(18)	0.8463(11)	0.48(2)
O(7)	4*a*	0.5039(10)	0.4508(17)	0.1027(16)	0.48(2)
O(8)	4*a*	0.5077(9)	0.7910(20)	0.9079(14)	0.48(2)
O(9)	4*a*	0.2039(16)	0.0657(18)	0.1961(13)	0.48(2)
O(10)	4*a*	0.8057(14)	0.7080(20)	0.3965(13)	0.48(2)
$LiFeSbO_5$ – space group *Pbn2₁* (#33)					
a = 14.2943(4) Å, *b* = 5.2771(1) Å, *c* = 9.5610(3) Å,					
volume = 721.21(4) Å³					
Radiation source: Synchrotron X-Ray, λ = 0.8268 Å					
Temperature: 298 K					
R_p = 2.01, R_{wp} = 1.40, R_{Bragg} = 1.03					

Table 2. Parameters from the structural refinement of $LiFeSbO_5$ against SXRD data collected at room temperature. The lithium positions are omitted due to their small X-ray scattering power. The *z*-coordinate of Sb(1) is fixed at 0 to 'anchor' the structure in this non-centrosymmetric space group.

^{57}Fe Mössbauer Spectroscopy. A ^{57}Fe Mössbauer spectrum collected from Li_2FeSbO_5 at room temperature can be satisfactorily fit by two doublets as shown in Figure 4 and detailed in Table 3. The chemical shift (CS) and quadrupole splitting (Δ) values of both doublets are consistent with tetrahedrally coordinated Fe^{3+}, and the spectrum of Li_2FeSbO_5 is very similar to that collected from Na_2FeSbO_5.[29] The requirement to use two doublets is attributed to a small amount of Li/Fe cation disorder in the phase which appears to be introduced in the cation exchange reaction.

A corresponding ^{57}Fe Mössbauer spectrum collected from $LiFeSbO_5$ at room temperature can also be fit by two doublets,

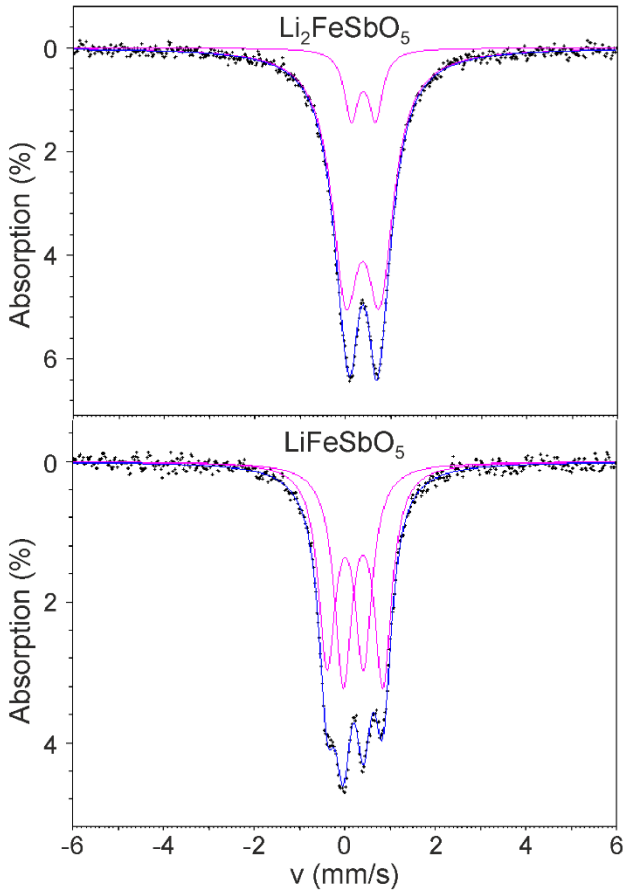

Figure 4. ^{57}Fe Mössbauer spectra collected from Li_2FeSbO_5 (top) and $LiFeSbO_5$ (bottom) at room temperature.

Li_2FeSbO_5				
	CS (mm/s) [±0.02]	Δ (mm/s) [±0.02]	HWHM (mm/s) [±0.02]	Spectral area (%) [± 2]
Doublet 1	0.39	0.76	0.37	87
Doublet 2	0.40	0.53	0.18	13
$LiFeSbO_5$				
	CS (mm/s) [±0.02]	Δ (mm/s) [±0.02]	HWHM (mm/s) [±0.02]	Spectral area (%) [± 2]
Doublet 1	0.01	0.80	0.23	47
Doublet 2	0.41	0.88	0.23	53

Table 3. Hyperfine parameters extracted from the fits to ^{57}Fe Mössbauer spectra. CS values are stated relative to α-Fe.

as shown in Figure 4 and detailed in Table 3. However, in this case the CS values of the two doublets are significantly different (0.01(2) mm/s and 0.41(2) mm/s) indicating the Fe^{4+} cations in $LiFeSbO_5$ have disproportionated into a 1:1 mixture of Fe^{3+} and Fe^{5+},[37, 38] in line with the different bond valence sums (Fe +4.04; Fe +2.09) calculated

for the two crystallographically distinct Fe sites in $LiFeSbO_5$ (Table S2) and the orange color of the material.

Magnetic Characterization. Zero-field cooled (ZFC) and field cooled (FC) magnetization data collected from Li_2FeSbO_5 as a function of temperature in an applied field of 100 Oe are shown in Figure 5. On cooling the ZFC and FC data diverge weakly below T = 275 K and then much more strongly below T = 75 K, with the ZFC data exhibiting a maximum at 65 K. The ZFC data do not obey the Curie-Weiss law over any temperature range measured. Magnetization-field data collected at 300 K are linear and pass through the origin, consistent with simple paramagnetic behavior. However, magnetization-field data collected at 5 K after cooling in an applied field of 50,000 Oe are sigmoidal and shifted above the origin, suggesting the divergence between ZFC and FC data at T = 75 K is the freezing of a spin glass.

ZFC and FC magnetization data collected from $LiFeSbO_5$ in an applied field of 100 Oe (Figure 6) obey the Curie-Weiss law ($\chi = C/(T-\theta)$) in the range $150 < T/K < 300$ to yield values of $C = 3.258(3)$ cm³ K mol⁻¹ and $\theta = -1.92(3)$ K. This value of the Curie constant is in good agreement with that expected for a 1:1 mixture of $S = {}^5/_2$ Fe^{3+} and $S = {}^3/_2$ Fe^{5+} ($C_{expected}$ = 3.125 cm³ K mol⁻¹) and is thus consistent with the disproportionation of Fe^{4+} to Fe^{3+} and Fe^{5+} indicated by the ^{57}Fe Mössbauer data. On cooling below T = 150 K the ZFC and FC data diverge weakly before exhibiting a maximum at T = 10 K. Magnetization-field data (Figure 6) are linear at 300 K, and weakly sigmoidal but centered on the origin at 5 K, increasing almost linearly with increasing field to achieve a value of ~0.8 μB per formula unit

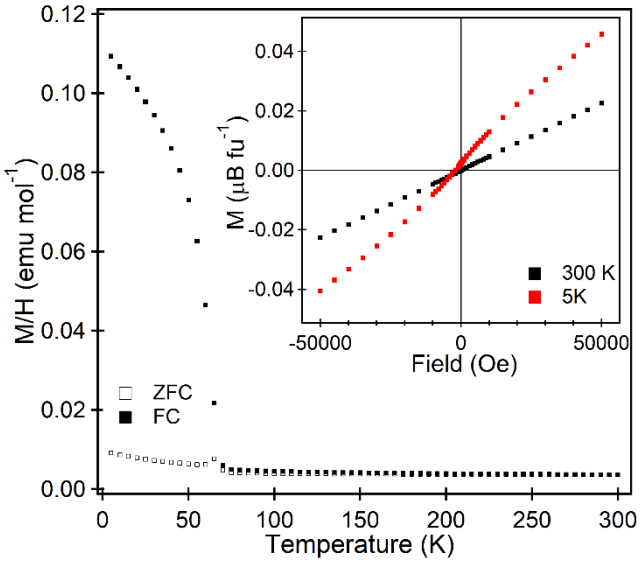

Figure 5. ZFC and FC data collected from Li_2FeSbO_5 as a function of temperature in an applied field of 100 Oe. Inset shows magnetization-field data collect at 300 K and 5 K after cooling in an applied field of 50,000 Oe.

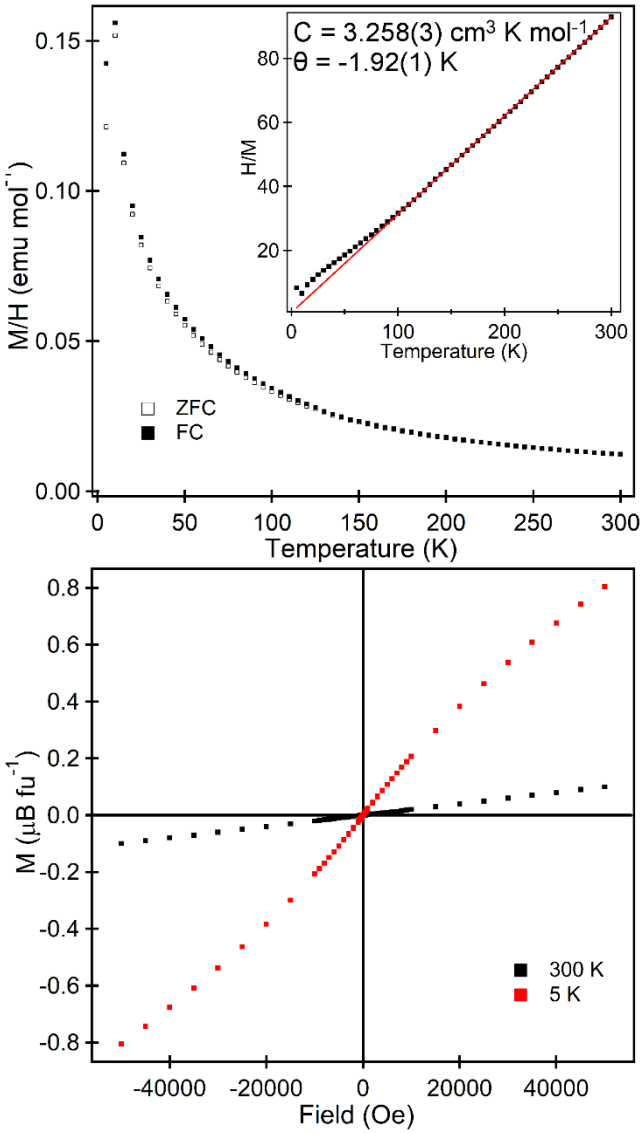

Figure 6. (top) ZFC and FC data collected from $LiFeSbO_5$ as a function of temperature in an applied field of 100 Oe. Inset shows fit to the Cure-Weiss law in the range $300 < T/K < 150$. (bottom) Magnetization-field data collect at 300 K and 5 K after cooling in an applied field of 50,000 Oe.

in 5T. This combination of features is rather unusual, and suggests an antiferromagnetic ground state for $LiFeSbO_5$ in small applied fields, which changes in an as-yet unidentified way as the applied filed increases.

Discussion

The structure of Na_2FeSbO_5 can be considered as a layered intergrowth of $Na_2Sb_2O_5$ sheets (structurally reminiscent of $LiSbO_3$), stacked with $Na_2Fe_2O_5$ sheets, (reminiscent of β-$NaFeO_2$), as shown in Figure 7. While the structures of both $LiSbO_3$ and β-$NaFeO_2$ are based on hexagonal close packed (hcp) arrays of oxide ions, the hcp stacking of the oxide-ion sheets is perturbed in Na_2FeSbO_5. The close packed sheets of oxide ions surrounding the $Na_2Sb_2O_5$ layers retain a close-packed arrangement (layers A and B in Figure 7). However, the sheets of oxide ions surrounding

the $Na_2Fe_2O_5$ layers (layers B and B') are related by a displacement along the *x*-axis, rather than having a close packed relationship. So the stacking sequence of the sheets of oxide ions is A(Na_2Sb_2)B(Na_2Fe_2)B'(Na_2Sb_2)A'(Na_2Fe_2)A as shown in Figure 7.

Lithium-for-sodium cation exchange yields Li_2FeSbO_5 which is isostructural with Na_2FeSbO_5. Replacement of the Na^+ cations with smaller Li^+ cations leads to an anisotropic contraction of the unit cell (Δvolume = -13.8%) which arises principally from a contraction along the *z*-axis (Δ*a* = -3.6%, Δ*b* = -3.5%, Δ*c* = -7.2%) and is accommodated by a flexing of the Sb-O-Fe and Fe-O-Fe bond angles, rather than a compression of the SbO_6 or FeO_4 units.

While the large contraction of the *c* lattice parameter can be directly attributed to the replacement of Na^+ with Li^+, the resulting torsion of the FeO_4 units leads to more complex consequences for the rest of the framework. Most notably there is a significant reduction in one of the separations between SbO_6 chains along the *x*-axis, which occurs at expense of a slight increase in the other, as shown in Figure 8. Furthermore the rotation of the FeO_4 units around the *y*-axis tightens the Fe-O-Fe bond angles, as shown in Figure 8, which is likely to be the cause of the reduction in the magnetic transition temperature of Li_2FeSbO_5 (75 K) compared to Na_2FeSbO_5 (104 K)[29] due to a weakening of superexchange interactions.

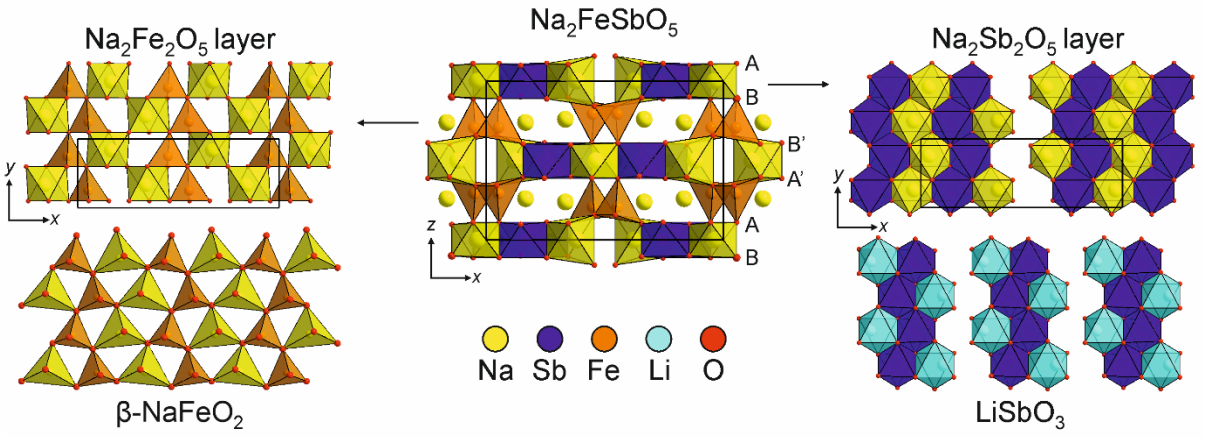

Figure 7. Structure of Na_2FeSbO_5 is an intergrowth of $Na_2Sb_2O_5$ layers (related to $LiSbO_3$) and $Na_2Fe_2O_5$ layers (related to β-$NaFeO_2$) with an A-B-B'-A'-A stacking sequence of close packed layers of oxide ions.

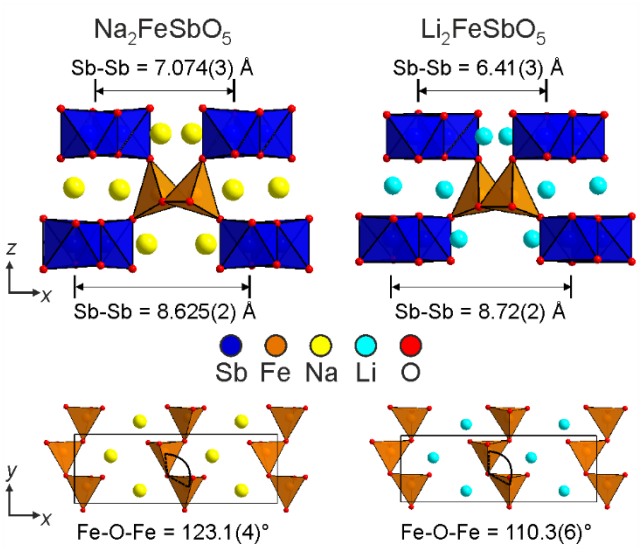

Figure 8. A comparison of the crystal structures of Na_2FeSbO_5 and Li_2FeSbO_5.

Deintercalation of one lithium per formula unit from Li_2FeSbO_5 leads to a large scale reorganization of the structure. As shown in Figure 9, the iron centers in $LiFeSbO_5$ are located in octahedral coordination sites which share edges to form zig-zag chains which run parallel to the *y*-axis.

The close-packed sheets of oxide ions which surround the iron-containing layers are now stacked in a close packed manner, so the stacking sequence of $LiFeSbO_5$ is A($LiSb_2$)B($LiFe_2$)A($LiSb_2$)B($LiFe_2$)A. This differs from the stacking sequence of Li_2FeSbO_5, revealing that on lithium deintercalation the $Li_{2-x}Sb_2O_5$ blocks slide relative to each other to generate octahedral coordination sites for the iron centers, which are occupied with a minor rearrangement of the Fe centers, to generate the structure shown in Figure 9. Similar shifting of close packed blocks has been observed during intercalation of lithium into layered, cation-deficient perovskite oxides, and other related reactions.[39] This large structural change observed on lithium removal is probably responsible for the apparent irreversibility of the chemical delithiation of Li_2FeSbO_5, as noted above.

Iron migration on charging/discharging has been observed in a number of other systems.[11, 18-20, 26] This behavior can be broadly attributed to the differing ionic radii and ligand-field stabilization energies of d^6 Fe^{2+}, d^5 Fe^{3+} and d^4 Fe^{4+}leading to differing coordination preferences for the different oxidation states of iron.

^{57}Fe Mössbauer data, supported by magnetic data, indicate that the nominally Fe^{4+} cations in $LiFeSbO_5$ disproportionate into a 1:1 ratio of Fe^{3+} and Fe^{5+}. Structural analysis

utilizing bond valence sums[40, 41], detailed in Table S2, suggests that charge-disproportionated Fe^{3+} and Fe^{5+} centers order crystallographically into chains containing either exclusively Fe^{3+} or Fe^{5+} which alternate along *x*- and *z*-axes as shown in Figure 9. This charge ordering pattern is rather unusual, as the majority of disproportionated $Fe^{3+/5+}$ systems adopt 3-dimensional 'rock-salt' or 2-dimensional 'checkerboard' arrangements of alternating Fe^{3+} and Fe^{5+} in order to minimize the electrostatic repulsions and lattice strain.[42-44] Nevertheless, the unusual charge ordering pattern present in $LiFeSbO_5$ seems to be very stable since charge disproportionated charges are found at room temperature. It is possible that the edge-sharing connectivity of the FeO_6 octahedra in $LiFeSbO_5$ (rather than the apex-linked connectivity more commonly observed in $Fe^{3+/5+}$ systems) could be responsible for the unusual ordering scheme, or that the phase is the product of a topochemical reaction and is thus far from equilibrium, unlike the majority of reported $Fe^{3+/5+}$ oxide phases.

As noted above, Fe^{4+} tends to be unstable in delitihated oxide phases,[18, 21, 23] so the observation of apparently stable Fe^{5+} centers in $LiFeSbO_5$ is notable as it demonstrates high oxidation states of iron can be stable in delithiated oxides, offering the prospect of preparing cathode materials which utilize the oxidation of Fe^{3+}. However, in this instance, the disproportionation of Fe^{4+} to Fe^{3+}/Fe^{5+} appears to drive a structural reorganization on the delithiation of Li_2FeSbO_5 making the oxidation irreversible, highlighting a further barrier to the development of high-voltage, high-capacity Fe-base cathode materials.

Conclusion

Facile Li-for-Na cation exchange readily converts Na_2FeSbO_5 to the metastable phase, Li_2FeSbO_5, with only a small relaxation of the structural framework. This Fe^{3+} phase can be chemically oxidized via delithiation with NO_2BF_4 to form $LiFeSbO_5$. The delithiation of Li_2FeSbO_5 is accompanied by a minor structural rearrangement of the $Li_{2-x}FeSbO_5$ sheets in the system, resulting in a change to the local iron coordination environment from tetrahedral in Li_2FeSbO_5 to octahedral in $LiFeSbO_5$. ^{57}Fe Mössbauer data and magnetization measurements indicate that the nominal Fe^{4+} centers in $LiFeSbO_5$ have disproportionated into a 1:1 combination of Fe^{3+} and Fe^{5+}. The structural rearrangement which occurs on oxidation can be attributed to the favorability of locating d^3 Fe^{5+} cations within octahedral rather than tetrahedral coordination sites, and represents a further undesirable feature (in addition to the apparent instability of Fe^{4+} in Li-Fe-X-O systems) which needs to be overcome if high-voltage, high-capacity, Fe-based cathode materials are to be developed.

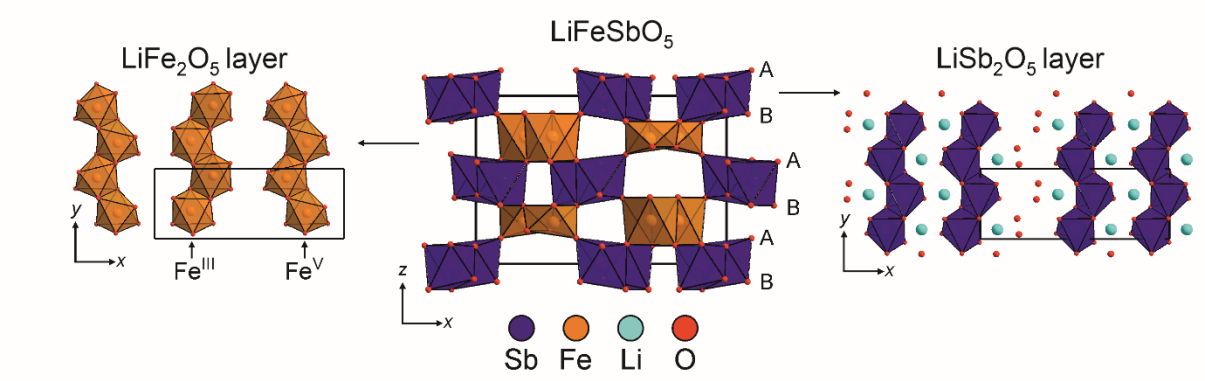

Figure 9. Structure of $LiFeSbO_5$ is an intergrowth of $LiSb_2O_5$ layers (related to $LiSbO_3$) and $LiFe_2O_5$ layers consisting of edge-sharing FeO_6 units, with an A-B-A-B hexagonal sequence of close packed layers of oxide ions.

ASSOCIATED CONTENT

Complete description of the compositional analysis of $LiFeSbO_5$. Selected bond lengths from the refined structures of Li_2FeSbO_5 and $LiFeSbO_5$.

AUTHOR INFORMATION

Corresponding Author

* michael.hayward@chem.ox.ac.uk

Author Contributions

The manuscript was written through contributions of all authors.

ACKNOWLEDGMENT

This work was supported by the Faraday Institution project FutureCat (Grant No. FIRG017). Experiments at the Diamond Light Source were performed as part of the Block Allocation Group award "Oxford Solid State Chemistry BAG to probe composition-structure-property relationships in solids" (CY25166).

References

1. Whittingham, M. S., Ultimate Limits to Intercalation Reactions for Lithium Batteries. *Chem. Rev.* **2014,** *114* (23), 11414-11443.

2. Liu, J.; Bao, Z. N.; Cui, Y.; Dufek, E. J.; Goodenough, J. B.; Khalifah, P.; Li, Q. Y.; Liaw, B. Y.; Liu, P.; Manthiram, A.; Meng, Y. S.; Subramanian, V. R.; Toney, M. F.; Viswanathan, V. V.; Whittingham, M. S.; Xiao, J.; Xu, W.; Yang, J. H.; Yang, X. Q.; Zhang, J. G., Pathways for practical high-energy long-cycling lithium metal batteries. *Nature Energy* **2019,** *4* (3), 180-186.

3. Whittingham, M. S., Lithium batteries and cathode materials. *Chem. Rev.* **2004,** *104* (10), 4271-4301.

4. Li, M.; Lu, J., Cobalt in lithium-ion batteries. *Science* **2020,** *367* (6481), 979-980.

5. Booth, S. G.; Nedoma, A. J.; Anthonisamy, N. N.; Baker, P. J.; Boston, R.; Bronstein, H.; Clarke, S. J.; Cussen, E. J.; Daramalla, V.; De Volder, M.; Dutton, S. E.; Falkowski, V.; Fleck, N. A.; Geddes, H. S.; Gollapally, N.; Goodwin, A. L.; Griffin, J. M.; Haworth, A. R.; Hayward, M. A.; Hull, S.; Inkson, B. J.; Johnston, B. J.; Lu, Z. H.; MacManus-Driscoll, J. L.; Labalde, X. M. D.; McClelland, I.; McCombie, K.; Murdock, B.; Nayak, D.; Park, S.; Perez, G. E.; Pickard, C. J.; Piper, L. F. J.; Playford, H. Y.; Price, S.; Scanlon, D. O.; Stallard, J. C.; Tapia-Ruiz, N.; West, A. R.; Wheatcroft, L.; Wilson, M.; Zhang, L.; Zhi, X.; Zhu, B. N.; Cussen, S. A., Perspectives for next generation lithium-ion battery cathode materials. *Apl Materials* **2021,** *9* (10), 109201.

6. Zhu, X. B.; Lin, T. G.; Manning, E.; Zhang, Y. C.; Yu, M. M.; Zuo, B.; Wang, L. Z., Recent advances on Fe- and Mn-based cathode materials for lithium and sodium ion batteries. *Journal of Nanoparticle Research* **2018,** *20* (6), 160.

7. Padhi, A. K.; Nanjundaswamy, K. S.; Goodenough, J. B., Phospho-olivines as positive-electrode materials for rechargeable lithium batteries. *J. Electrochem. Soc.* **1997,** *144* (4), 1188-1194.

8. Li, J. G.; Li, J. J.; Luo, J.; Wang, L.; He, X. M., Recent Advances in the LiFeO2-based Materials for Li-ion Batteries. *International Journal of Electrochemical Science* **2011,** *6* (5), 1550-1561.

9. Kanno, R.; Shirane, T.; Kawamoto, Y.; Takeda, Y.; Takano, M.; Ohashi, M.; Yamaguchi, Y., Synthesis, structure, and electrochemical properties of a new lithium iron oxide, $LiFeO_2$, with a corrugated layer structure. *J. Electrochem. Soc.* **1996,** *143* (8), 2435-2442.

10. Wang, M. J.; Navrotsky, A., $LiMO_2$ (M = Mn, Fe, and Co): Energetics, polymorphism and phase transformation. *J. Solid State Chem.* **2005,** *178* (4), 1230-1240.

11. Abdel-Ghany, A. E.; Mauger, A.; Groult, H.; Zaghib, K.; Julien, C. M., Structural properties and electrochemistry of alpha-$LiFeO_2$. *Journal of Power Sources* **2012,** *197*, 285-291.

12. Sakurai, Y.; Arai, H.; Yamaki, J., Preparation of electrochemically active alpha-$LiFeO_2$ at low temperature. *Solid State Ionics* **1998,** *113*, 29-34.

13. Morales, J.; Santos-Pena, J., Highly electroactive nanosized alpha-$LiFeO_2$. *Electrochemistry Communications* **2007,** *9* (8), 2116-2120.

14. Barre, M.; Catti, M., Neutron diffraction study of the beta ' and gamma phases of $LiFeO_2$. *J. Solid State Chem.* **2009,** *182* (9), 2549-2554.

15. Guo, S. P.; Ma, Z.; Li, J. C.; Xue, H. G., First investigation of the electrochemical performance of gamma-$LiFeO_2$ micro-cubes as promising anode material for lithium-ion batteries. *J. Mater. Sci.* **2017,** *52* (3), 1469-1476.

16. Kanno, R.; Shirane, T.; Inaba, Y.; Kawamoto, Y., Synthesis and electrochemical properties of lithium iron oxides with layer-related structures. *Journal of Power Sources* **1997,** *68* (1), 145-152.

17. Shirane, T.; Kanno, R.; Kawamoto, Y.; Takeda, Y.; Takano, M.; Kamiyama, T.; Izumi, F., Structure and Physical-Properties of Lithium Iron-Oxide, $LiFeO_2$, Synthesized by Ionic Exchange-Reaction. *Solid State Ionics* **1995,** *79*, 227-233.

18. Armstrong, A. R.; Tee, D. W.; La Mantia, F.; Novak, P.; Bruce, P. G., Synthesis of tetrahedral $LiFeO_2$ and its behavior as a cathode in rechargeable lithium batteries. *J. Am. Chem. Soc.* **2008,** *130* (11), 3554-3559.

19. Lee, Y. S.; Sato, S.; Sun, Y. K.; Kobayakawa, K.; Sato, Y., A new type of orthorhombic $LiFeO_2$ with advanced battery performance and its structural change during cycling. *Journal of Power Sources* **2003,** *119*, 285-289.

20. Lee, Y. S.; Sato, S.; Tabuchi, M.; Yoon, C. S.; Sun, Y. K.; Kobayakawa, K.; Sato, Y., Structural change and capacity loss mechanism in orthorhombic Li/$LiFeO_2$ system during cycling. *Electrochemistry Communications* **2003,** *5* (7), 549-554.

21. Hirayama, M.; Tomita, H.; Kubota, K.; Kanno, R., Structure and electrode reactions of layered rocksalt $LiFeO_2$ nanoparticles for lithium battery cathode. *Journal of Power Sources* **2011,** *196* (16), 6809-6814.

22. Catti, M.; Montero-Campillo, M., First-principles modelling of lithium iron oxides as battery cathode materials. *Journal of Power Sources* **2011,** *196* (8), 3955-3961.

23. Bordet-Le Guenne, L.; Deniard, P.; Lecerf, A.; Biensan, P.; Siret, C.; Fournes, L.; Brec, R., Intrinsic instability of Fe^{4+} in electrochemically oxidized ramsdellite and orthorhombic $Li_{1-x}H_xFeO_2$. *J. Mater. Chem.* **1999,** *9* (5), 1127-1134.

24. Lebens-Higgins, Z.; Chung, H.; Temprano, I.; Zuba, M.; Wu, J. P.; Rana, J.; Mejia, C.; Jones, M. A.; Wang, L.; Grey, C. P.; Du, Y. G.; Yang, W. L.; Meng, Y. S.; Piper, L. F. J., Electrochemical Utilization of Iron IV in the $Li_{1.3}Fe_{0.4}Nb_{0.3}O_2$ Disordered Rocksalt Cathode. *Batteries & Supercaps* **2021,** *4* (5), 771-777.

25. Luo, M. Z.; Zheng, S. Y.; Wu, J.; Zhou, K.; Zuo, W. H.; Feng, M.; He, H. J.; Liu, R.; Zhu, J. P.; Zhao, G.; Chen, S. J.; Yang, W. L.; Peng, Z. Q.; Wu, Q. H.; Yang, Y., Identifying the anionic redox activity in cation-disordered $Li_{1.25}Nb_{0.25}Fe_{0.5}oO_2$/C oxide cathodes for Li-ion batteries *Journal of Materials Chemistry A* **2020,** *8* (27), 13852-13852.

26. Masese, T.; Tassel, C.; Orikasa, Y.; Koyama, Y.; Arai, H.; Hayashi, N.; Kim, J.; Mori, T.; Yamamoto, K.; Kobayashi, Y.; Kageyama, H.; Ogumi, Z.; Uchimoto, Y., Crystal Structural Changes and Charge Compensation Mechanism during Two Lithium Extraction/Insertion between Li_2FeSiO_4 and $FeSiO_4$. *Journal of Physical Chemistry C* **2015,** *119* (19), 10206-10211.

27. McCalla, E.; Abakumov, A.; Rousse, G.; Reynaud, M.; Sougrati, M. T.; Budic, B.; Mahmoud, A.; Dominko, R.; Van Tendeloo, G.; Hermann, R. P.; Tarascon, J. M., Novel Complex Stacking of Fully-Ordered Transition Metal Layers in Li_4FeSbO_6 Materials. *Chem. Mater.* **2015,** *27* (5), 1699-1708.

28. McCalla, E.; Sougrati, M. T.; Rousse, G.; Berg, E. J.; Abakumov, A.; Recham, N.; Ramesha, K.; Sathiya, M.; Dominko, R.; Van Tendeloo, G.; Novak, P.; Tarascon, J. M., Understanding the Roles of Anionic Redox and Oxygen Release during Electrochemical Cycling of Lithium-Rich Layered Li_4FeSbO_6. *J. Am. Chem. Soc.* **2015,** *137* (14), 4804-4814.

29. Uma, S.; Vasilchikova, T.; Sobolev, A.; Raganyan, G.; Sethi, A.; Koo, H. J.; Whangbo, M. H.; Presniakov, I.; Glazkova, I.; Vasiliev, A.; Streltsov, S.; Zvereva, E., Synthesis and Characterization of Sodium-Iron Antimonate Na_2FeSbO_5: One-Dimensional Antiferromagnetic Chain Compound with a Spin-Glass Ground State. *Inorg. Chem.* **2019,** *58* (17), 11333-11350.

30. Politaev, V. V.; Nalbandyan, V. B., Subsolidus phase relations, crystal chemistry and cation-transport properties of sodium iron antimony oxides. *Solid State Sci.* **2009,** *11* (1), 144-150.

31. Wizansky, A. R.; Rauch, P. E.; Disalvo, F. J., Powerful oxidizing-agents for the oxidative deintercalation of lithium from transition-metal oxides. *J. Solid State Chem.* **1989,** *81* (2), 203-207.

32. Coelho, A. A. *TOPAS Academic: General profile and Structure Analysis Software For Powder Diffraction Data*, Bruker AXS, Karlsruhe, Germany: 2016.

33. Lagarec, K.; G., R. D. *Recoil: Mössbauer spectral analysis software for windows*, 1998.

34. Sears, V. F., Neutron Scattering Lengths and Cross Sections. *Neutron News* **1992,** *3*, 26-37.

35. Campbell, B. J.; Stokes, H. T.; Tanner, D. E.; Hatch, D. M., ISODISPLACE: a web-based tool for exploring structural distortions. *J. Appl. Crystallogr.* **2006,** *39*, 607-614.

36. Stokes, H. T.; Hatch, D. M.; Campbell, B. J. *ISOTROPY Software Suite*, iso.byu.edu, 2007.

37. Takeda, Y.; Naka, S.; Takano, M.; Shinjo, T.; Takada, T.; Shimada, M., Preparation and characterization of stoichiometric $CaFeO_3$. *Mater. Res. Bull.* **1978,** *13* (1), 61-66.

38. Yamada, I.; Takata, K.; Hayashi, N.; Shinohara, S.; Azuma, M.; Mori, S.; Muranaka, S.; Shimakawa, Y.; Takano, M., A perovskite containing quadrivalent iron as a charge-disproportionated ferrimagnet. *Angew. Chem., Int. Ed.* **2008,** *47* (37), 7032-7035.

39. Perejon, A.; Hayward, M. A., Reductive lithium insertion into B-cation deficient niobium perovskite oxides. *Dalton Trans.* **2015,** *44* (23), 10636-10643.

40. Brese, N. E.; O'Keeffee, M., Bond-Valence Parameters for Solids. *Acta Crystallogr., Sect. B : Strucut. Sci.* **1991,** *B47*, 192-197.

41. Brown, I. D.; Altermatt, D., Bond-Valence Parameters Obtained from a Systematic Analysis of the Inorganic Crystal Structure Database. *Acta Crystallogr., Sect. B : Strucut. Sci.* **1985,** *B41*, 244-247.

42. Ganesanpotti, S.; Tassel, C.; Hayashi, N.; Goto, Y.; Bouilly, G.; Yajima, T.; Kobayashi, Y.; Kageyama, H., Charge Disproportionation and Magnetoresistivity in a Double Perovskite with Alternate Fe^{4+} d^4 and Mn^{4+} d^3 Layers. *European Journal of Inorganic Chemistry* **2014,** (15), 2576-2581.

43. Hosaka, Y.; Ichikawa, N.; Saito, T.; Manuel, P.; Khalyavin, D.; Attfield, J. P.; Shimakawa, Y., Two-Dimensional Charge Disproportionation of the Unusual High Valence State Fe^{4+} in a Layered Double Perovskite. *J. Am. Chem. Soc.* **2015,** *137* (23), 7468-7473.

44. Woodward, P. M.; Cox, D. E.; Moshopoulou, E.; Sleight, A. W.; Morimoto, S., Structural studies of charge disproportionation and magnetic order in $CaFeO_3$. *Phys. Rev. B* **2000,** *62* (2), 844-855.

SYNOPSIS TOC